RADIATION RESEARCH **194**, 587–593 (2020)
0033-7587/20 $15.00

DOI: 10.1667/RADE-19-00015.1

Ultra-High Dose-Rate, Pulsed (FLASH) Radiotherapy with Carbon Ions: Generation of Early, Transient, Highly Oxygenated Conditions in the Tumor Environment

Abdullah Muhammad Zakaria,[a] Nicholas W. Colangelo,[b,1] Jintana Meesungnoen,[a] Edouard I. Azzam,[b,2] Marc-Émile Plourde[a] and Jean-Paul Jay-Gerin[a,3]

[a] *Département de Médecine Nucléaire et de Radiobiologie, Faculté de Médecine et des Sciences de la Santé, Université de Sherbrooke, Sherbrooke, Canada; and* [b] *Rutgers Biomedical and Health Sciences, New Jersey Medical School, Department of Radiology, Newark, New Jersey*

Zakaria, A. M., Colangelo, N. W., Meesungnoen, J., Azzam, E. I., Plourde, M-É. and Jay-Gerin, J-P. Ultra-High Dose-Rate, Pulsed (FLASH) Radiotherapy with Carbon Ions: Generation of Early, Transient, Highly Oxygenated Conditions in the Tumor Environment. *Radiat. Res.* 194, 587–593 (2020).

It is well known that molecular oxygen is a product of the radiolysis of water with high-linear energy transfer (LET) radiation, which is distinct from low-LET radiation wherein O_2 radiolytic yield is negligible. Since O_2 is a powerful radiosensitizer, this fact is of practical relevance in cancer therapy with energetic heavy ions, such as carbon ions. It has recently been discovered that large doses of ionizing radiation delivered to tumors at very high dose rates (i.e., in a few milliseconds) have remarkable benefits in sparing healthy tissue while preserving anti-tumor activity compared to radiotherapy delivered at conventional, lower dose rates. This new method is called "FLASH radiotherapy" and has been tested using low-LET radiation (i.e., electrons and photons) in various pre-clinical studies and recently in a human patient. Although the exact mechanism(s) underlying FLASH are still unclear, it has been suggested that radiation delivered at high dose rates spares normal tissue via oxygen depletion. In addition, heavy-ion radiation achieves tumor control with reduced normal tissue toxicity due to its favorable physical depth-dose profile and increased radiobiological effectiveness in the Bragg peak region. To date, however, biological research with energetic heavy ions delivered at ultra-high dose rates has not been performed and it is not known whether heavy ions are suitable for FLASH radiotherapy. Here we present the additive or even synergistic advantages of integrating the FLASH dose rates into carbon-ion therapy. These benefits result from the ability of heavy ions at high LET to generate an oxygenated microenvironment around their track due to the occurrence of multiple (mainly double) ionization of water. This oxygen is abundant immediately in the tumor region where the LET of the carbon ions is very high, near the end of the carbon-ion path (i.e., in the Bragg peak region). In contrast, in the "plateau" region of the depth-dose distribution of ions (i.e., in the normal tissue region), in which the LET is significantly lower, this generation of molecular oxygen is insignificant. Under FLASH irradiation, it is shown that this early generation of O_2 extends evenly over the entire irradiated tumor volume, with concentrations estimated to be several orders of magnitude higher than the oxygen levels present in hypoxic tumor cells. Theoretically, these results indicate that FLASH radiotherapy using carbon ions would have a markedly improved therapeutic ratio with greater toxicity in the tumor due to the generation of oxygen at the spread-out Bragg peak.

INTRODUCTION

Theoretically, all types of malignant tumors could be eradicated if treated with sufficiently high doses of radiation. However, radiation also damages normal tissue making normal tissue toxicity the main limitation in the administration of curative radiation doses in cancer treatment (*1*). In FLASH radiation therapy (FLASH-RT), ultra-high dose rates are used to deliver large doses of radiation to tumors almost instantaneously (a few milliseconds), while unexpectedly sparing normal tissue (*2*, *3*). Recently published work reporting on this relative protection of normal tissues sparked great interest in the use of FLASH for cancer treatment. However, there exists a lack of understanding of the underlying mechanism(s) of this effect (*4*).

For more than 50 years, dose-rate effects have been an important topic in radiobiology and radiotherapy (*5*, *6*). Since fundamental radiobiological processes, even if they are numerous and complex, are commonly triggered in an aqueous environment, a thorough knowledge of the radiation chemistry of water is essential in addressing this topic. Indeed, pulsed radiation in water radiolysis has been useful in identifying the short-term chemical species that trigger the biological consequences of radiation exposure. In

[1] Scholar-in-training, Radiation Research Society.
[2] Address for correspondence: Department of Radiology, New Jersey Medical School, 205 South Orange Ave., Room F1212, Newark, NJ 07103; email: edouard.azzam@rutgers.edu.
[3] Email: jean-paul.jay-gerin@usherbrooke.ca.

particular, it has been shown that in ~1 ps after initial energy deposition, radiolytic products formed in pure, deaerated water, exposed to either low- or high-linear energy transfer (LET) radiation, include the hydrated electron (e^-_{aq}), $H^\bullet$, H_2, $^\bullet OH$, H_2O_2, H_3O^+ and OH^-, among others (*7*, *8*). In an aerobic cellular environment under normal irradiation conditions (i.e., low absorbed dose rate), e^-_{aq} and $H^\bullet$ atoms produced in localized spurs or tracks are scavenged by dissolved molecular oxygen on a time scale of a few microseconds (assuming a typical intracellular O_2 concentration of ~30 μ*M*) and converted to superoxide anions ($O_2^{\bullet-}$) and hydroperoxyl ($HO_2^\bullet$) radicals, respectively. At physiological pH, $HO_2^\bullet$ dissociates to $O_2^{\bullet-}$ [$pK_a(HO_2^\bullet/O_2^{\bullet-}) \approx 4.8$ in water at 25°C] (*9*). In contrast to the relatively low dose rates used in conventional therapeutic irradiations, the energy of the ionizing radiation can be considered as evenly distributed over the *entire* irradiated volume in ultra-high-dose-rate FLASH (*10*). In this case, the overall physicochemical situation changes significantly due to the overlap between the adjacent spurs or tracks, which occur quickly after the absorption of the radiation. This interaction between neighboring spurs and tracks results in an increased initial concentration of radicals (e^-_{aq}, $H^\bullet$ and $^\bullet OH$), comparable to, or even higher than that of intracellular O_2. Under these conditions, *radical-radical combination reactions* in which molecular products are formed (mainly H_2O_2 and H_2O, H_2 being relatively inert) are favored, and the effect of *radiolytic oxygen depletion* (*or consumption*) becomes important (*1*, *2*, *10*). Translated to basic cellular radiobiological research, both of these mechanisms could significantly reduce radiation effects and thus explain the protection of normal tissues in FLASH-RT (*4*, *11–16*). Finally, worthy of mention here is a third mechanism that was recently advanced, which could also play a role in FLASH, namely the generation of early, transient, strongly *acidic pH spikes* that result from the formation of hydronium ions (H_3O^+) during the initial stages of water radiolysis (*17*, *18*).

Currently used in several countries (notably Japan and Germany), carbon ions have a characteristic dose deposition profile in which energy is released inversely to the velocity of the ions (*19*, *20*). Therapeutically, the carbon ions enter tissue at a high energy (e.g., ~290 MeV/nucleon) and an LET in the lower range (~13 keV/μm for 290 MeV/nucleon $^{12}C^{6+}$), but they deposit energy as they penetrate the tissue, which leads to their having less energy and a higher LET, particularly towards the end of their path. They therefore deliver a lower entry dose and deposit most of their energy in the tumor near the end of the flight path (the ''Bragg peak''). In other words, if the Bragg peak occurs in the tumor, there is potential for increased sparing of the normal tissue. A similar dose distribution is not possible with low-LET conventional irradiation methods. Radiobiologically, carbon ions are also two- to threefold more effective at killing cells than protons and conventional radiation modalities (*21*). Moreover, compared to photon radiation, carbon ions produce complex DNA damage that is not easily repaired, and cells exposed to carbon ions have a lower ''oxygen enhancement ratio'' (OER) and are less affected by variations in radiosensitivity related to the cell cycle (*22*). Compared to protons, they also have a higher LET and lower lateral dose distribution. In short, carbon ions improve tumor cell killing compared to conventional photons or protons at a given dose of radiation. Determining whether carbon ions delivered at ultra-high dose rates can provide clinically relevant FLASH-RT could dramatically improve cancer management (*23*). It may also accelerate the development of laser acceleration for heavy ions, which could be delivered at dose rates of $\sim 10^{11}$ Gy/s (*24*), as it may be difficult to achieve the necessary dose rates with current carbon-ion therapy facilities.

While FLASH-RT has been studied in the context of electron, photon and proton therapies, the efficacy of heavy ions, such as energetic carbon ions, under FLASH conditions remains unclear (*23*). Regardless of the radiation modality, basic biology experiments and clinical trials will be required to demonstrate the safety and efficacy of FLASH radiotherapy. However, physicochemical modeling can help describe the underlying mechanisms by which FLASH radiotherapy achieves its beneficial effects, and may suggest whether these ultra-high-dose-rate techniques would be favorable in the context of carbon-ion therapy. Here, based on pure radiation chemistry, we present the additive or even synergistic advantages of integrating the FLASH dose rates into therapy with energetic heavy ions, using the example of carbon ions. These benefits result from the ability of heavy ions at high LET to generate an oxygenated microenvironment around their track [for low-LET radiation, O_2 is not considered to be a primary radiolytic product (*7*, *8*)], due to the occurrence of multiple (mainly double) ionization of water (*25–28*). This early O_2 generation is shown to occur preferentially in the Bragg peak region where the LET of carbon ions is highest. In carbon-ion therapy, this Bragg peak region is targeted to the tumor volume.

Here, we sought to determine how the physicochemical changes occurring under FLASH dose rates may alter oxygen generation for irradiations with energetic carbon ions. We use Monte Carlo track chemistry simulations of the radiolysis of pure, deaerated water to calculate the early yields (or *G* values) and concentrations of O_2 for irradiating carbon ions of different initial energies, with and without the inclusion of the mechanism of multiple ionization of water molecules at 25°C. A brief presentation of our simulation approach is given below.

MONTE CARLO TRACK CHEMISTRY SIMULATION

The carbon-ion radiolysis of pure, deaerated liquid water at high LET was modeled using our Monte Carlo track chemistry simulation code IONLYS-IRT. A detailed description of this code has been provided elsewhere [see (*26*) and references therein]. In short, the sequence of all

individual stochastic events of the early physical ($<10^{-15}$ s) and physicochemical ($\sim10^{-15}$–10^{-12} s) stages in the track development is handled by our IONLYS event-by-event simulation program. The energy deposition by the multiply-charged incident ion and by all secondary electrons generated by it takes place through the slowing down of these particles. This is done via a variety of elastic and inelastic scattering processes and thus by generating a large number of ionized and electronically excited water molecules. To take into account the effects of direct multiple ionization of the outer (loosely bound) electron shells of the target under the impact of high-LET heavy ions, the model incorporates double and triple ionization processes in single ion-water collisions. Ionizations of higher multiplicity are neglected since they are much less likely to occur in the LET range of interest here. Theoretically, it is difficult to acquire a detailed description of multiple ionization, due to the complex, quantum-mechanical many-body nature of the scattering mechanisms involved. Nevertheless, some attempts have been made to simulate the role of multiple ionization in liquid water to assess its consequences for the heavy-ion radiation chemistry of water [for a review, see (*25*)]. The carbon-ion cross-section values that were used for the double and triple ionizations of water in our track structure simulation modeling have been described in detail elsewhere (*25–28*) and are therefore not discussed further here.

The consequences of multiple ionization with two, three or more outgoing electrons in the final state have often not been considered in the models of water radiation chemistry and biology. Yet, this hypothesis goes back to Platzman (*29*), who came to the conclusion more than 60 years ago that these processes, although rare compared to single ionization events, should be ''*extremely effective chemically*'' due to the high instability of the multiply-ionized molecules produced. Only recently has this earlier hypothesis been reconsidered to explain the production of $HO_2^{\bullet}$/$O_2^{\bullet-}$ that has been experimentally observed in heavy-ion radiolysis of water at high LET (*30–32*).

Little, in fact, is known about the fate of multiply-ionized water molecules *in solution*. Here, the rearrangement of these thermodynamically unstable charged water cations is treated according to the general mechanism proposed by Ferradini and Jay-Gerin (*30*), which assumes that, in liquid water, H_2O^{n+} ($n = 1$–10; the molecule of water has 10 bound electrons) dissociates by *acid-base re-equilibration processes* [see Table 14.3 of (*25*)]. Among these processes, it is assumed that the chemical production of O_2 (mainly) results from the *doubly*-ionized water molecules through the intervention of oxygen atoms formed in their ^3P ground state, according to the overall dissociation reaction (*28*):

$$H_2O^{2+} + 2H_2O \rightarrow 2H_3O^+ + O(^3P), \quad (1)$$

followed by

$$O(^3P) + O(^3P) \rightarrow O_2 \quad (2)$$

or

$$O(^3P) + {}^{\bullet}OH \rightarrow HO_2^{\bullet} \quad (3)$$

$$HO_2^{\bullet} + O(^3P) \rightarrow O_2 + {}^{\bullet}OH, \quad (4)$$

at a very early stage in the expansion of the tracks. We should recall here that the $O(^3P)$ atoms in the ground state are rather inert to water and, due to the *very high-local concentration of radicals*, react efficiently with themselves or with $^{\bullet}OH$ in the heavy-ion track core (*26*, *30*). As for the *triple*-charged water cations, we have:

$$H_2O^{\bullet 3+} + 4H_2O \rightarrow 3H_3O^+ + HO_2^{\bullet}. \quad (5)$$

The complex spatial distribution of reactants at the end of the physicochemical stage, which is provided as an output of the IONLYS program, is then used directly as the starting point for the ''chemical stage'' ($>10^{-12}$ s). This third stage, in which the different radiolytic species diffuse and react with themselves or with dissolved solutes (if any) present at the time of irradiation, is covered by our IRT program. This program uses the ''independent reaction times'' (IRT) method (*33*) to model chemical development in this stage and to simulate the formation of measurable yields. It is a computer-efficient stochastic simulation technique that simulates reaction times without having to follow the trajectories of the diffusing species. The IRT method is based on the approximation that the reaction time of each pair of reactants is independent of the presence of other reactants in the system. Its detailed implementation has previously been described elsewhere [see (*26*) and references therein]. The reaction scheme and parameters used in our IRT program for pure liquid water at 25°C are the same as those used previously, as described elsewhere [see Table 1 in (*34*)], except that they now include some newly measured or recently reevaluated reaction rates by Elliot and Bartels (*35*). The values for the diffusion coefficients of the various reactive species involved in the simulations are listed elsewhere [see table 6 in (*36*)].

The O_2 yields generated by the radiolysis of liquid water were calculated as a function of time in the interval $\sim10^{-12}$ to 10^{-6} s for three representative incident carbon-ion energies, namely, 4.1, 290 and 400 MeV/nucleon. This was done by simulating short ($\sim$2–40 μm) carbon-ion track segments, over which the energy and LET of the ion are well defined and remain nearly constant. Typically, approximately 5,000 to 4×10^5 reactive chemical species are generated during the chemical development of these simulated track segments (depending on the LET), whereby the average chemical yields can be calculated with acceptable statistical reliability.

RESULTS AND DISCUSSION

Figure 1 shows the time profiles of $G(O_2)$ at 25°C, over the range of $\sim10^{-12}$–10^{-6} s, obtained from our Monte Carlo

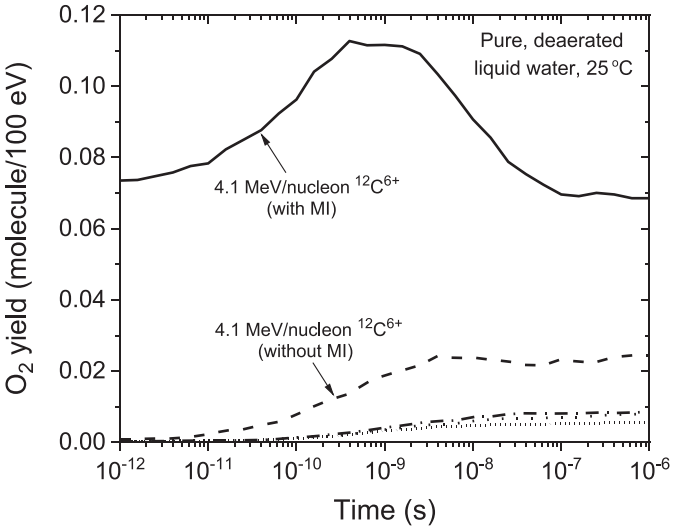

FIG. 1. Time dependence of the O_2 yields calculated from our IONLYS-IRT Monte Carlo track chemistry simulations of the radiolysis of pure, air-free liquid water at 25°C, in the interval of 10^{-12}–10^{-6} s, for the three incident carbon ions considered here: 4.1 (with and without multiple ionization of water molecules), 290 and 400 MeV per nucleon (LET: ~330, 11.3, and 10 keV/μm, respectively). Note that multiple ionization plays no significant role on the values of $G(O_2)$ for the lower-LET 290 and 400 MeV/nucleon $^{12}C^{6+}$ ions (represented by dash-dot and dot-dot lines, respectively). The short-dot line corresponds to our calculated $G(O_2)$ values for 300-MeV protons (which mimic the low-LET limiting case of ^{60}Co γ or fast electron irradiation, LET ~ 0.3 keV/μm) and is shown here for comparison. Radiation chemical yields are expressed in units of molecule per 100 eV. For conversion into SI units (mol/J), 1 molecule/100 eV ≈ 0.10364 μmol/J (*7*, *8*). MI = multiple ionization.

track chemistry simulations (with or without multiple ionization of water) for the three irradiating carbon ions: 4.1, 290 and 400 MeV/nucleon (LET ~ 330, 11.3 and 10 keV/μm, respectively). The O_2 yield for 300-MeV protons, which mimic the low-LET limiting case of ^{60}Co γ or fast-electron irradiation (LET ~0.3 keV/μm) (*28*), is also shown in the figure for comparison. As can be seen, these yields remain low in the absence of multiple ionization of water, with $G(O_2)$ showing only a slight gradual increase with increasing LET, similar to the other molecular yields of the radiolysis (*7*, *8*). In contrast, our calculations show that $G(O_2)$ increases sharply considering the mechanism of multiple ionization of water. This is clearly shown in Fig. 1 for 4.1 MeV/nucleon $^{12}C^{6+}$ ions, i.e., for the highest LET studied, where $G(O_2)$ increases early (~10^{-12} s) from ~0.0009 molecule/100 eV in the absence of multiple ionization to ~0.074 molecule/100 eV when multiple ionization is included in the simulations (an increase of approximately two orders of magnitude). Interestingly, the curve of $G(O_2)$ reaches a maximum of ~0.113 molecule/100 eV around 4×10^{-10} s, after which it drops to finally stabilize at approximately 0.068 molecule/100 eV at 1 μs.

Using the G values for O_2 obtained from our Monte Carlo simulations, we can estimate the corresponding oxygen concentrations of the ion track as a function of time, using the general relationship $C = \rho DG$, where C is the concentration of species, ρ is the density, D is the radiation dose and G is the chemical yield (*37*). In fact, assuming that the oxygen molecules are generated evenly in axially homogeneous cylinders with a length of L = 1 μm and initial radius r_c equal to the radius of the physical ''core'' of the impacting ion tracks (at ~10^{-13} s) (*38*, *39*), the track concentrations of O_2 can be derived from (*17*, *26*):

$$[O_2] \approx G(O_2) \times \left(\frac{\mathrm{LET}}{\pi r(t)^2} \right), \tag{6}$$

where

$$r(t)^2 \approx r_c^2 + 4Dt \tag{7}$$

represents the change with time of r_c due to the two-dimensional (2D) diffusive expansion of the tracks. Here, t is the time and D is the diffusion coefficient of O_2 [$D = 2.42 \times 10^{-9}$ m^2/s at 25°C (*40*)]. r_c corresponds to the tiny radial region within the first few nanometers around the ion trajectories. In this study, an r_c of ~2 nm was assumed for the three carbon ions under consideration (*26*, *28*). Figure 2 shows typical 3D representations of track segments of a 300-MeV/nucleon carbon ion (LET ~ 10 keV/μm), 4.1-MeV/nucleon carbon ion (LET ~ 330 keV/μm), and a 300-MeV proton (LET ~ 0.3 keV/μm) traversing through liquid water using calculations from our IONLYS simulation code. As is evident here, the energy density of the deposition in the core area is very high for the high-LET 4.1-MeV/nucleon $^{12}C^{6+}$ ions.

Figure 3 shows the time profiles of the O_2 concentrations (referred to as $[O_2]$) at 25°C in the three considered carbon-ion tracks, 4.1, 290 and 400 MeV/nucleon in the interval of ~10^{-12}–10^{-6} s, calculated directly from Eqs. (6) and (7) using the $G(O_2)$ values given in Fig. 1 (with and without multiple ionization of water). For comparison purposes, the figure also shows the corresponding values of $[O_2]$ for 300-MeV incident protons (*28*). As shown, carbon ions with higher LET lead to increased production of nascent oxygen compared to those with lower LET over the studied time range. Interestingly, our results for the 4.1-MeV/nucleon $^{12}C^{6+}$ ions (LET ~ 330 keV/μm) showed a steep increase in the values of $[O_2]$ when the multiple ionization of water molecules was incorporated compared to those obtained in the absence of multiple ionization. For example, the initial value of $[O_2]$ (at ~10^{-12} s) increases from ~0.4 to 32.2 mM when the multiple ionization of water is included in the calculations. This value is approximately three orders of magnitude higher than the oxygen levels in most normal human cells (~30 μM), and *a fortiori* in normally oxygenated tumor regions (which vary considerably, from zero to more than 20 μM) as well as in hypoxic tumor regions (a large part of which have almost no oxygenation) (*22*, *28*, *41*, *42*). The results found in Fig. 3 also show that, for the 290- and 400-MeV/nucleon $^{12}C^{6+}$ ions (i.e., of much lower LET, ~11.3 and 10 keV/μm, respectively), the O_2 concentrations generated are significantly lower, not more

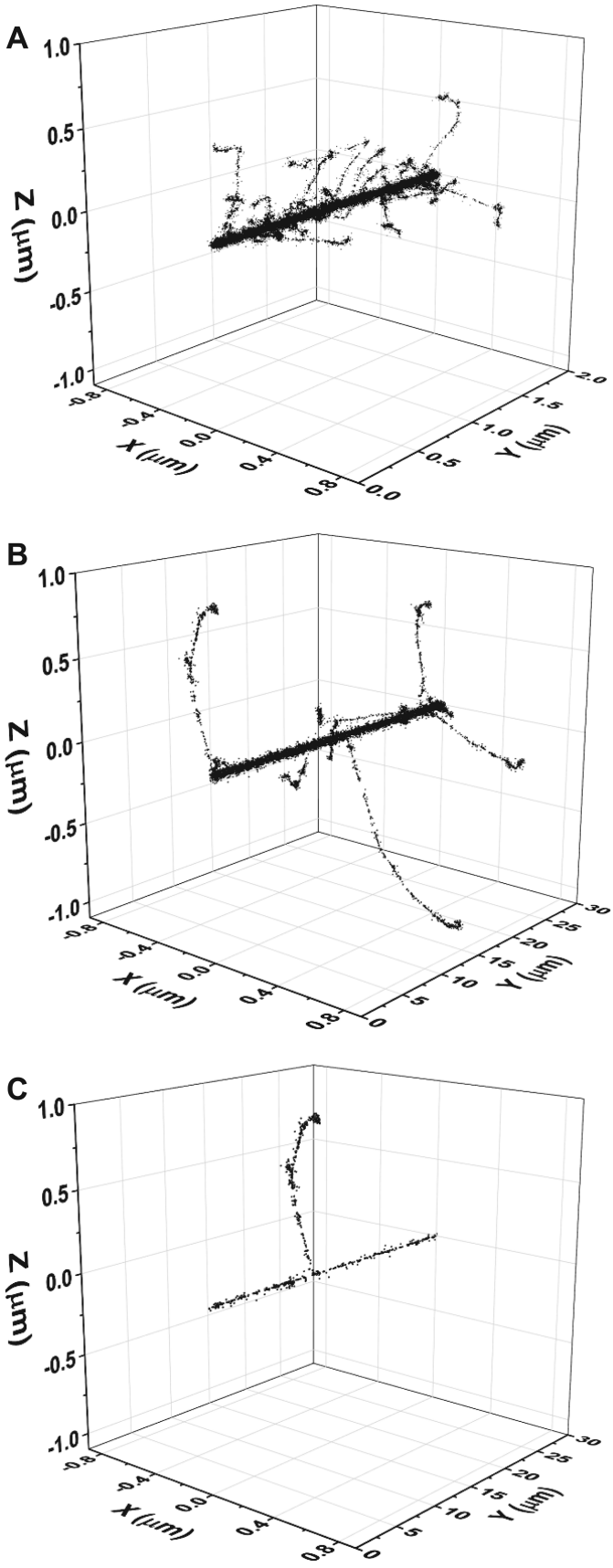

FIG. 2. Three-dimensional representations of track segments for the following impacting ions: (panel A) 4.1-MeV/nucleon $^{12}C^{6+}$ (LET ~ 330 keV/μm, 2-μm track length), (panel B) 300-MeV/nucleon $^{12}C^{6+}$ (LET ~ 11 keV/μm, 30-μm track length), and (panel C) 300-MeV $^{1}H^{+}$ (LET ~ 0.3 keV/μm, 30-μm track length) traversing through liquid water at 25°C, calculated (at ~10^{-13} s) with our IONLYS Monte Carlo simulation code. Ions are generated at the origin and start traveling along the y-axis. Each dot represents an interaction where energy deposition occurred. Surrounding the ''core'' of the track is a much larger region (named the ''penumbra'') in which all of the energy is deposited by energetic secondary electrons (δ rays) that result from knock-on collisions with the primary carbon ion.

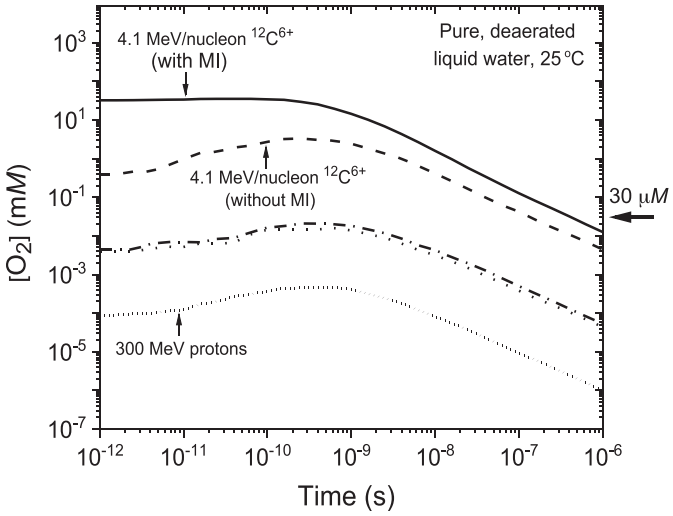

FIG. 3. Time dependence of the corresponding track concentrations of O_2 (in m*M*) (with and without multiple ionization of water molecules) calculated as explained in the text for the three incident carbon ions under consideration, using the $G(O_2)$ values reported in Fig. 1. As in Fig. 1, the $[O_2]$ values for the lower-LET 290 and 400 MeV/nucleon $^{12}C^{6+}$ ions are represented by the dash-dot and dot-dot lines, respectively. The short-dot line corresponds to our calculated $[O_2]$ values for 300-MeV protons (which mimic the low-LET limiting case of ^{60}Co γ or fast electron irradiation, LET ~ 0.3 keV/μm), shown in the figure for comparison. Typical O_2 concentrations in normal human cells (~30 μ*M*) are indicated by the arrow on the right side. MI = multiple ionization.

than ~20 μ*M* (at ~4×10^{-10} s). Our results clearly show a substantial production of ''radiolytic'' molecular oxygen in the tracks of high-LET carbon ions immediately after the passage of the ion. Interestingly, however, this level of O_2 production is *not* observed in low-LET-irradiating ions.

To understand the role of FLASH ultra-high dose rates with energetic heavy ions, we must first recall the change in LET with the penetration depth of the ions. This is shown in Fig. 4 for the three irradiating carbon ions studied. As mentioned above, the energy distribution of carbon ions over the treatment field is highly inhomogeneous. Carbon ions deliver a lower entry dose (i.e., in the ''plateau'' region where the LET is rather low) and deposit most of their energy towards the end of their flight path (i.e., at the Bragg peak, where they have their highest LET). Clinically, carbon-ion radiotherapy is performed in such a way that the Bragg peak is contained in the tumor, resulting in a therapeutic index superior to conventional photon irradiation and a reduction in toxicity to normal tissue.

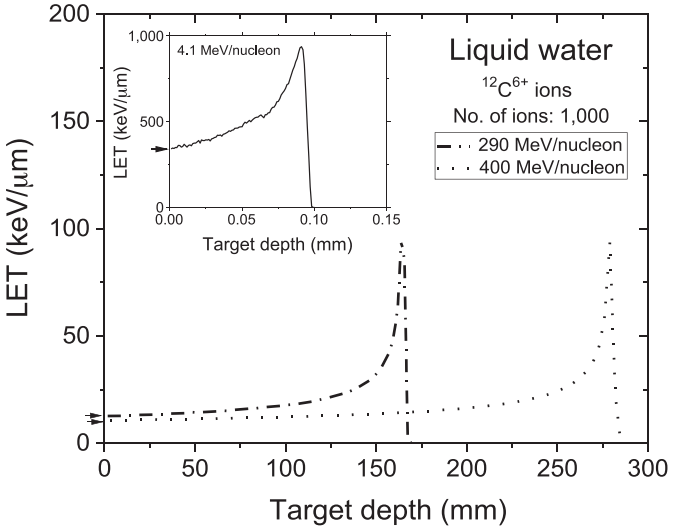

FIG. 4. Changes in LET with the penetration depth in liquid water at 25°C for carbon ions at the three energies considered in this study, as obtained using the SRIM software (*43*). Total ions calculated = 1,000. The arrows on the left side show the entry LET of the ions: ~330, 11.3 and 10 keV/μm, corresponding to the incident ion energies of 4.1, 290 and 400 MeV per nucleon, respectively.

It is well established that molecular oxygen can be a strong radiation sensitizer (*22*, *44*) with the biological response to radiation being greater under oxygenated conditions than under hypoxic conditions. The radiolytic formation of O_2 (due to the occurrence of multiple ionization of water) in the Bragg peak (i.e., in the tumor region), where the LET of the carbon ions is very high, should therefore convert initially hypoxic (i.e., radioresistant) tumor cells into an ''oxygenated'' environment around the relevant cellular target molecules, which leads to a strong improvement in cell killing (*22*, *45*). In contrast, this level of oxygen generation would *not* occur in normal tissue because it is in the ''plateau'' region of the depth-dose distribution of ions where the LET is lower (see Fig. 4).

In the context of FLASH irradiation used to date [e.g., instantaneous dose rates of ~10^6–10^7 Gy/s were used by Favaudon *et al*. (*2*)], the average distance between adjacent tracks is small enough that they overlap to a certain degree at early times (*10*, *18*). Under these conditions, the energy of the impinging carbon ions can be considered as being relatively evenly distributed over the irradiated volume. In that case, the early, transient generation of O_2 at the Bragg peak described above should thus occur in all track regions and then, due to their close proximity, extend *evenly* over the *entire* irradiated tumor volume. Radiobiologically, this highly oxygenated environment throughout the entire tumor volume should considerably improve tumor cell killing by causing damage from which cancer cells cannot recover.

Taken together, our results provide critical insights into the additive or even synergistic benefits of combining carbon-ion therapy with FLASH-RT, not only to eliminate tumors but also to protect surrounding normal tissues and thus alleviate potential long-term adverse effects.

CONCLUSION

This study highlights the potential biological effect of nascent oxygen formation associated with heavy ions at ultra-high dose rates. This is of particular importance for improving assessment of the clinical potential of FLASH-RT with heavy ions. It has been shown that FLASH, using low-LET electrons, is a promising new method that damages the tumor while protecting normal tissue. Here we found that ultra-high-dose-rate carbon ions increasingly generate molecular oxygen towards the end of their trajectory at the Bragg peak, which is located within the tumor in clinical radiotherapy with heavy ions. This finding indicates increased cell killing potential through the use of carbon ions. Taken together, our results suggest with the use of energetic carbon-ion FLASH-RT, an even better therapeutic ratio can be achieved due to the creation of an oxygenated environment in the tumor, which contributes to increased cell killing efficacy while simultaneously protecting normal tissue.

ACKNOWLEDGMENTS

AMZ is the recipient of a scholarship from the ''Programme de Bourses d'excellence aux études supérieures'' of the Université de Sherbrooke. Financial support was also provided by the National Institutes of Health (NIH grant no. F30CA206389 to NWC), the National Aeronautics and Space Administration (NASA grant no. NNX15AD62G to EIA) and the Natural Sciences and Engineering Research Council of Canada (NSERC grant no. RGPIN-2015-06100 to JP J-G).

Received: December 11, 2019; accepted: June 26, 2020; published online: August 27, 2020

REFERENCES

1. Bernier J, Hall JE, Giaccia A. Radiation oncology: A century of achievements. Nat Rev Cancer 2004; 4:737–47.
2. Favaudon V, Caplier L, Monceau V, Pouzoulet F, Sayarath M, Fouillade C, et al. Ultrahigh dose-rate FLASH irradiation increases the differential response between normal and tumor tissue in mice. Sci Transl Med 2014; 6:245ra93.
3. Favaudon V, Fouillade C, Vozenin M-C. Ultrahigh dose-rate, ''flash'' irradiation minimizes the side-effects of radiotherapy. Cancer Radiother 2015; 19:526–31.
4. Favaudon V. Flash radiotherapy at very high dose-rate: A brief account of the current situation. Cancer Radiother 2019; 23:674–6.
5. Hall EJ. Radiation dose-rate: A factor of importance in radiobiology and radiotherapy. Br J Radiol 1972; 45:81–97.
6. Hall EJ, Brenner DJ. The dose-rate effect revisited: radiobiological considerations of importance in radiotherapy. Int J Radiat Oncol Biol Phys 1991; 21:1403–14.
7. Ferradini C, Jay-Gerin J-P. Radiolysis of water and aqueous solutions: history and current events. (Article in French). Can J Chem 1999; 77:1542–75.
8. Spinks JWT, Woods RJ. An introduction to radiation chemistry, 3rd ed. New York: Wiley; 1990.
9. Azzam EI, Jay-Gerin J-P, Pain D. Ionizing radiation-induced metabolic oxidative stress and prolonged cell injury. Cancer Lett 2012; 327:48–60.
10. Kuppermann A. Diffusion kinetics in radiation chemistry. In: Haïssinsky M, editor. Actions chimiques et biologiques des radiations. Paris: Masson; 1961. p. 85–166.

11. Dewey DL, Boag JW. Modification of the oxygen effect when bacteria are given large pulses of radiation. Nature (London) 1959; 183:1450–1.

12. Epp ER, Weiss H, Ling CC. Irradiation of cells by single and double pulses of high intensity radiation: oxygen sensitization and diffusion kinetics. Curr Top Radiat Res Q 1976; 11:201–50.

13. Wilson P, Jones B, Yokoi T, Hill M, Vojnovic B. Revisiting the ultra-high dose rate effect: implications for charged particle radiotherapy using protons and light ions. Br J Radiol 2012; 85:e933–9.

14. Spitz DR, Buettner GR, Petronek MS, St-Aubin JJ, Flynn RT, Waldron TJ, et al. An integrated physico-chemical approach for explaining the differential impact of FLASH versus conventional dose rate irradiation on cancer and normal tissue responses. Radiother Oncol 2019; 139:23–7.

15. Pratx G, Kapp DS. A computational model of radiolytic oxygen depletion during FLASH irradiation and its effect on the oxygen enhancement ratio. Phys Med Biol 2019; 64:185005.

16. Montay-Gruel P, Acharya M, Petersson K, Alikhani L, Yakkala C, Allen BD, et al. Long-term neurocognitive benefits of FLASH radiotherapy driven by reduced reactive oxygen species. Proc Natl Acad Sci U S A 2019; 116:10943–51.

17. Kanike V, Meesungnoen J, Jay-Gerin J-P. Acid spike effect in spurs/tracks of the low/high linear energy transfer radiolysis of water: potential implications for radiobiology. RSC Adv 2015; 5:43361–70.

18. Jay-Gerin J-P. Ultra-high dose-rate (FLASH) radiotherapy: generation of early, transient, strongly acidic spikes in the irradiated tumor environment. Cancer Radiother 2020; 24:332–4.

19. Schardt D, Elsässer T, Schulz-Ertner D. Heavy-ion tumor therapy: Physical and radiobiological benefits. Rev Mod Phys 2010; 82:383–425.

20. Ebner DK, Kamada T. The emerging role of carbon-ion radiotherapy. Front Oncol 2016; 6:140.

21. Mohamad O, Sishc BJ, Saha J, Pompos A, Rahimi A, Story MD, et al. Carbon ion radiotherapy: a review of clinical experiences and preclinical research, with an emphasis on DNA damage/repair. Cancers 2017; 9:66.

22. Hall EJ, Giaccia AJ. Radiobiology for the radiologist. 6th ed. Philadelphia: Lippincott Williams and Wilkins; 2006.

23. Colangelo NW, Azzam EI. The importance and implications of FLASH ultrahigh dose rates for protons and heavy ions. Radiat Res 2019; 193:1–4.

24. Karsch L, Beyreuther E, Enghardt W, Gotz M, Masood U, Schramm U, et al. Towards ion beam therapy based on laser plasma accelerators. Acta Oncologica 2017; 56:1359–66.

25. Meesungnoen J, Jay-Gerin J-P. Radiation chemistry of liquid water with heavy ions: Monte Carlo simulation studies. In: Hatano Y, Katsumura Y, Mozumder A, editors. Charged particle and photon interactions with matter. Recent advances, applications, and interfaces. Boca Raton: CRC Press (Taylor and Francis Group); 2011. p. 355–400.

26. Meesungnoen J, Jay-Gerin J-P. High-LET radiolysis of liquid water with 1H+, 4He2+, 12C6+, and 20Ne9+ ions: effects of multiple ionization. J Phys Chem A 2005; 109:6406–19.

27. Meesungnoen J. Effect of multiple ionization on the radiolysis of liquid water irradiated with heavy ions: A theoretical study using Monte-Carlo simulations. PhD Thesis, Université de Sherbrooke, Sherbrooke, Canada; 2007. (https://bit.ly/3eLPp6Z)

28. Meesungnoen J, Jay-Gerin J-P. High-LET ion radiolysis of water: oxygen production in tracks. Radiat Res 2009; 171:379–86.

29. Platzman RL. On the primary processes in radiation chemistry and biology. In: Nickson JJ, editor. Symposium on radiobiology. The basic aspects of radiation effects on living systems. New York: Wiley; 1952. p. 97–116.

30. Ferradini C, Jay-Gerin J-P. Does multiple ionization intervene for the production of HO2. radicals in high-LET liquid water radiolysis? Radiat Phys Chem 1998; 51:263–7.

31. Meesungnoen J, Filali-Mouhim A, Snitwongse Na Ayudhya N, Mankhetkorn S, Jay-Gerin J-P. Multiple ionization effects on the yields of HO2./O2.– and H2O2 produced in the radiolysis of liquid water with high-LET 12C6+ ions: a Monte Carlo simulation study. Chem Phys Lett 2003; 377:419–25.

32. Gervais B, Beuve M, Olivera GH, Galassi ME, Rivarola RD. Production of HO_2 and O_2 by multiple ionization in water radiolysis by swift carbon ions. Chem Phys Lett 2005; 410:330–4.

33. Pimblott SM, Pilling MJ, Green NJB. Stochastic models of spur kinetics in water. Radiat Phys Chem 1991; 37:377–88.

34. Mirsaleh Kohan L, Sanguanmith S, Meesungnoen J, Causey P, Stuart CR, Jay-Gerin J-P. Self-radiolysis of tritiated water. 1. A comparison of the effects of 60Co g-rays and tritium b-particles on water and aqueous solutions at room temperature. RSC Adv 2013; 3:19282–99.

35. Elliot AJ, Bartels DM. The reaction set, rate constants and g-values for the simulation of the radiolysis of light water over the range 20 deg to 350 deg C based on information available in 2008. AECL Report No. 153-127160-450-001. Chalk River, Canada: Atomic Energy of Canada Limited; 2009.

36. Tippayamontri T, Sanguanmith S, Meesungnoen J, Sunaryo GR, Jay-Gerin J-P. Fast neutron radiolysis of the ferrous sulfate (Fricke) dosimeter: Monte Carlo simulations. Vol. 10. In: Pandalai SG, editor. Recent research developments in physical chemistry. Trivandrum, Kerala, India: Transworld Research Network; 2009. p. 143–211.

37. Hummel A. Radiation chemistry: the chemical effects of ionizing radiation and their applications. Delft: Interfaculty Reactor Institute-Technische Universiteit Delft (IRI-DUT); 1995.

38. Magee JL, Chatterjee A. Track reactions of radiation chemistry. In: Freeman GR, editor. Kinetics of nonhomogeneous processes. New York: Wiley; 1987. p. 171–214.

39. Mozumder A. Fundamentals of radiation chemistry. San Diego, CA: Academic Press; 1999.

40. Lide DR, editor. CRC Handbook of chemistry and physics. 85th ed. Boca Raton, FL: CRC Press; 2003.

41. Pogue BW, O'Hara JA, Wilmot CM, Paulsen KD, Swartz HM. Estimation of oxygen distribution in RIF-1 tumors by diffusion model-based interpretation of pimonidazole hypoxia and Eppendorf measurements. Radiat Res 2001; 155:15–25.

42. Halliwell B, Gutteridge JMC. Free radicals in biology and medicine. 5th ed. Oxford: Oxford University Press; 2015.

43. Ziegler JF, Bierdack JP, Ziegler MD. SRIM – The stopping and range of ions in matter. Chester, MD: SRIM Co.; 2015.

44. Gray LH, Conger AD, Ebert M, Hornsey S, Scott OCA. The concentration of oxygen dissolved in tissues at the time of irradiation as a factor in radiotherapy. Br J Radiol 1953; 26:638–48.

45. von Sonntag C. Free-radical-induced DNA damage and its repair. A chemical perspective. Berlin: Springer-Verlag; 2006.